Journal of Photochemistry & Photobiology, B: Biology 178 (2018) 428–439

Contents lists available at ScienceDirect

Journal of Photochemistry & Photobiology, B: Biology

journal homepage: www.elsevier.com/locate/jphotobiol

New platinum (II) and palladium (II) complexes of coumarin-thiazole Schiff base with a fluorescent chemosensor properties: Synthesis, spectroscopic characterization, X-ray structure determination, in vitro anticancer activity on various human carcinoma cell lines and computational studies

Ömer Şahin[a], Ümmühan Özmen Özdemir[a,*], Nurgül Seferoğlu[b], Zuhal Karagöz Genc[c], Kerem Kaya[d], Burcu Aydıner[a], Suat Tekin[e], Zeynel Seferoğlu[a]

[a] Department of Chemistry, Faculty of Science, Gazi University, Teknikokullar, Ankara 06500, Turkey
[b] Department of Advanced Technology, Gazi University, Teknikokullar, Ankara 06500, Turkey
[c] Adıyaman University, Metallurgy and Materials Engineering, Adıyaman 2230, Turkey
[d] Department of Chemistry, Faculty of Science and Letters, Istanbul Technical University, Istanbul 34469, Turkey
[e] Department of Physiology, Faculty of Medicine, Inonu University, Malatya, Turkey

ARTICLE INFO

Keywords:
Schiff base
Coumarin-thiazole
Fluorescent chemosensor
Platinum (II) and palladium (II) complexes
Anticancer activity
Anion sensitivity

ABSTRACT

A new coumarin-thiazole based Schiff base (**Ligand**, **L**) and its Pd(II), Pt(II) complexes; ([Pd(L)$_2$] and [Pt(L)$_2$]), were synthesized and characterized using spectrophotometric techniques (NMR, IR, UV–vis, LC-MS), magnetic moment, and conductivity measurements. **A** single crystal X-ray analysis for only **L** was done. The crystals of **L** have monoclinic crystal system and P21/c space group. To gain insight into the structure of **L** and its complexes, we used density functional theory (DFT) method to optimize the molecules. The photophysical properties changes were observed after deprotonation of **L** with CN^- via intermolecular charge transfer (ICT). Additionally, as the sensor is a colorimetric and fluorimetric cyanide probe containing active sites such as coumarin-thiazole and imine (CH = N), it showed fast color change from yellow to deep red in the visible region, and yellow fluorescence after CN^- addition to the imine bond, in DMSO. The reaction mechanisms of **L** with CN^-, F^- and AcO^- ions were evaluated using ^{1}H NMR shifts. The results showed that, the reaction of **L** with CN^- ion was due to the deprotonation and addition mechanisms at the same time. The anti-cancer activity of **L** and its Pd(II) and Pt(II) complexes were evaluated in vitro using MTT assay on the human cancer lines MCF-7 (human breast adenocarcinoma), LS174T (human colon carcinoma), and LNCAP (human prostate adenocarcinoma). The anti-cancer effects of **L** and its complexes, on human cells, were determined by comparing the half maximal inhibitory concentration (IC_{50}) values. The activity results showed that, the Pd(II) complex of **L** has higher anti-tumor effect than **L** and its Pt(II) complex against the tested human breast adenocarcinoma (MCF-7), human prostate adenocarcinoma (LNCAP), and human colon carcinoma (LS174T) cell lines.

1. Introduction

The heterocyclic compounds bearing coumarin derivatives have importance in organic and medicinal chemistry for many years, as a large number of natural products [1]. They are generally used as food additives, perfumes, cosmetics, pharmaceuticals [2], optical brighteners [3], fluorescent and laser dyes [4]. Coumarin derivatives have anti-coagulant effect and some coumarin drugs (warfarin and acenocoumarol) have wide usage as anticoagulants [5,6]. Especially, their physiological, anti-bacterial and anti-tumor activities make them vital therapeutic drugs for further medical treatments. Weber has reported that, coumarin and its metabolite nomenclatured as 7-hydroxycoumarin have anti-tumor activities against some human tumor cells [7]. Coumarin derivatives are potent tumor inhibitors of cellular proliferation in various cancer types [8–10]. In addition, it has been reported that, 4-hydroxycoumarin and 7-hydroxycoumarin inhibit the cell growth in gastric carcinoma cell line [11]. The heterocyclic compounds containing coumarin-thiazole hybrid system exhibit enhanced antimicrobial activities against different pathogens [12], including *Mycobacterium tuberculosis* [13] and *Helicobacter pylori* [14]. It is known that, such compounds have also good anti-cancer, anti-inflammatory, anti-analgesic, and anti-cholinesterase activity [15–17]. Moreover

* Corresponding author.
E-mail address: ummuhan@gazi.edu.tr (Ü.Ö. Özdemir).

https://doi.org/10.1016/j.jphotobiol.2017.11.030
Received 21 June 2017; Received in revised form 19 November 2017; Accepted 20 November 2017
Available online 22 November 2017
1011-1344/

Schiff bases containing coumarin-thiazole moiety are expected to have strong antitumor and other biological activites [18–20]. In addition, metal complexes of coumarin derivatives showed significant antitumor [21], antimicrobial activity [22,23] and anticoagulant activity [24].

Transition metal complexes as antitumor agents have been extensively used following the success of *cis*-platin. Recently, *cis*-platin has been identified as one of the most widely used antitumor drugs in the world, high effectivity for testicular and ovarian cancers, in the treatment of oropharyngeal, bronchogenic, cervical, and bladder carcinoma species [25]. Platinum complexes are clinically used to aid the inducement of cancer cells death. However, despite the positive effects of platinum compounds in killing cancer cells, they have also toxic effects [26]. To overcome these disadvantages, thousands of platinum complexes were synthesized and tested for their anticancer activities [27–29]. Organonitrile Pt(II) complexes and *cis*- and *trans*-[$PtCl_2$-$(NCR)_2$] (R = Me, Ph) were synthesized for promising Pt(II)-based cancer drugs. The cytotoxic properties of these Pt(II) complexes were evaluated with respect to cell growth inhibition against different types of human cancer cell lines [30]. Among the non-platinum compounds being used for cancer treatment, Palladium (II) derivatives have antitumor activity as much as the *cis*-platin drug, while they exhibit less kidney toxicity [31,32]. Therefore, new Palladium complexes that can be promising for the development of novel and advanced chemotherapic agents are in need. There are many structural similarities between Palladium and Platinum complexes relative to their biological effects as antitumor drugs [33]. The comparisons between these two metal complexes in terms of their cytotoxic activities are oftentimes made. The chemotherapeutic activities of various Palladium and Platinum complexes have been compared against different cancer cells and it was reported that Palladium complexes were more effective [34].

In our previous study, we reported the anion selectivity and sensitivity study of chemosensor based coumarin-thiazole containing Schiff base. And also we synthesized its Pt(II) and Pd(II) complexes [35]. In current study, we report new Schiff base (**L**) bearing coumarin-thiazole hybrid and its Pt(II)/Pd(II) complexes, which have been synthesized and characterized by using spectrometric techniques such as NMR, IR, LC–MS, UV–vis, magnetic moment, molar conductivity, as well as X-ray diffraction method. The chemosensing performance of **L** towards some anions was intestigated by using spectroscopic methods. The anticancer activities of all the synthesized compounds were evaluated on MCF-7, LNCAP, LS174T cell lines by comparing with the IC_{50} values. The DFT and TD-DFT calculations were performed to get more information and support the experimental results.

2. Experimental

2.1. Materials and Methods

Reagents, anions and solvents used in all steps of the synthesis and measurements were procured from Sigma Aldrich USA, and used as commercial grade without further purification. All reaction products were controlled by TLC using Merck silica gel (60 F254) plates (0.25 mm) and UV light. Infrared spectra were recorded on a Mattson 1000 FT-IR spectrophotometer. Nuclear magnetic resonance ($^1H/^{13}C$ NMR/anion titration) spectra were recorded on a Bruker Ultrashield 300 MHz NMR spectrometer. UV–vis absorption spectra were recorded on an Analytikjena Specord 200 Spectrophotometer. Flourescence properties were investigated by using HITACHI F-7000 FL Spectrofluorophotometer. All melting points were measured by Electrothermal 9200 melting point apparatus. LC-MS spectra was taken with Waters LCT Premier XE (LC-MS) mass spectrometer (Ankara University, Laboratories, Department of Pharmacological Sciences, Turkey). The magnetic moments of metal complexes were measured on powdered samples using Gouy method. To determine the ionic nature of the complexes, the molar conductivities were measured by Siemens WPA CM 35 conductometer. The cytotoxic effects of synthesized compounds against human cancer cells (breast, prostate and colon carcinoma) were analyzed by MTT assay method [36].

2.2. Synthesis of Ligand (L)

L having modified coumarin with thiazole ring were synthesized by using our previous method [35].

To a mixture of 2-amino-4-(3-coumarinyl)thiazole (15 mmol, 0.36 g) and 2-hydroxy-5-methylbenzaldehyde (15 mmol, 0.204 g) in 30 mL of ethanol, 3–5 drops of piperidine were added to the reaction mixture and refluxed for 6 h. The crude yellow product was washed with water and ethanol, and dried in in vacuum. The dark yellow crystals were isolated from ethanol-acetic acid mixture, and was collected in 65% yield (0.335 g); m.p: 211 °C; FT-IR (KBr, cm^{-1}): 3046 (Arom. C—H), 2922 (Aliph. C—H), 1714 (C═O, lactone), 1605 (C═C), 1564 (C═N) 1272 (C—O); ^1H NMR (DMSO-d_6, 300 MHz) δ: 11.25 (s, 1H); 9.33 (s, 1H); 8.86 (s; 1H); 8.35 (s, 1H); 7.98 (dd, *J*: 1.3, 7.95 Hz, 1H); 7.70 (dt, *J*: 1.5, 8.5 Hz, 1H); 7.66 (d, *J*: 6.6, 1H); 7.63 (t, *J*: 7.7, 1H); 7.43 (s, 1H); 7.31 (dd, *J*:1.3, 8.1, 1H); 6.65 (t, *J*:8.0, 1H); 2.40 (s, 3H); ^{13}C NMR (DMSO-d_6, 100 MHz) δ: 171.1; 167.8; 164.6; 153.1; 153.0; 150.0; 146.2; 146.2; 138.6; 137.7; 136.5; 132.6; 129.6; 125.3; 120.5; 119.6; 117.6; 116.4; 109.2; 20.2. LC-MS ES +, m/z = 363.0811.

2.3. Synthesis of PdL_2 and PtL_2 Complexes

To a heated solution of **L** (1 mmol) in 25 mL of ethanol, metal chlorides (Na_2PdCl_4 and K_2PtCl_4) (0.5 mmol) in 2 mL of water were added dropwise in 1:2 (M:L) molar ratio in basic media (with NaOH). The reaction mixtures were refluxed for two days on magnetic stirrer. The resulting pale brown precipitate were washed with water/ethanol/ether and left in glass oven at 150 °C for a 2 h in vacuum and left in a desiccator over $CaCl_2$ to prevent hydration and kept dried. Yield: 63% (Pd(II) complex), Yield: 40% (Pt(II) complex). $Pd(L)_2$: FT-IR (KBr, cm-1): 3046 (Arom. C—H), 2922 (Aliph. C—H), 1716 (C═O, lactone), 1605 (C═C), 1535 (C═N) 1249 (C—O). $Pt(L)_2$: FT-IR (KBr, cm-1): 3046 (Arom. C—H), 2923 (Aliph. C—H), 1716 (C═O, lactone), 1697(C═C), 1570 (C═N) 1258 (C—O).

2.4. UV–vis and Fluorimetric Studies of L with Different Anions

2.4.1. UV–vis and Fluorimetric Titration

L (0.0036 mg, 1×10^{-5} mol) was dissolved in DMSO (1 mL, 1×10^{-2} M), and 1×10^{-2} M of **L** were diluted to 1×10^{-3} M. Tetrabutylammonium (TBA) salts of each of the anions (TBAX) (1 mol) was dissolved in DMSO (1 mL, 1×10^{-2} M). 60 μL of **L** and 1940 μL DMSO (For fluorimetric titration, thus, 20 μL of **L** (1×10^{-3} M) and 1980 μL DMSO were taken) were measured and poured into the glass cell for the final concentration of 3×10^{-5} M. 2–40 μL of TBA solution (1×10^{-2}) were added to each **L** solution (3×10^{-5}) prepared above, into the glass cell. After shaking for a short time, UV–vis spectra were taken at room temperature (25 °C). TBA salts of Cl^-, Br^-, I^-, CN^-, OAc^-, $H_2PO_4^-$, NO_3^-, HSO_4^- and F^- (1×10^{-2}) were dissolved in 1 mL of DMSO. In this experimental part, all changes in UV–vis and emission spectra of **L** were detected during each TBA salt additions, while the concentration of **L** was fixed at 3×10^{-5} M for UV–vis titration, and 1×10^{-5} M for fluorimetric titration.

2.4.2. ^1H NMR Titration

For ^1H NMR titrations, two stock solutions were prepared in DMSO-d_6, one containing **L** (1×10^{-2} M) only, and the other containing an appropriate concentration of each of the following ions, F −, AcO − and CN − (1 M). Aliquots of the two solutions were mixed directly in NMR tubes. The NMR sample temperature was kept at 25 °C.

2.5. X-Ray Diffraction Method

The crystal structure of **L** was evaluated by Bruker D8 VENTURE diffractometer equipped with PHOTON100 detector using graphite monochromated Mo-Kα radiation (λ = 0.71073 Å) and scanned with 1.0° Φ-rotation frames at 100 Kelvin using Bruker Kryoflex II cooling attachment. The crystal structure was determined by intrinsic method SHELXS-1997 (Sheldrick, 1997) [37] and refined SHELXL-2014/7 (Sheldrick, 2008) [38]. Molecular drawings were generated using OLEX2. Ver. 1.2-dev [39]. The single crystal and instrumental parameters, further details on data collection and refinements are exhibited in the supporting information file. CCDC 1472133 contains the supplementary crystal data of **L** for this paper.

2.6. Theoretical Calculations for L and its Metal Complexes

All theoretical studies were computed with the Gaussian 09 program package [40] at the B3LYP computational level [41,42]. The initial geometry of the molecule was obtained from X-ray results and optimized in gas phase using the 6–311 + G(d,p) basis set, without including any symmetry constraints. In the calculations, LANL2DZ basis set was used for Pd(II)/Pt(II) complexes, whereas the 6–311 + G(d,p) basis set for Schiff base. ^{1}H NMR shifts were computed by the gauge including atomic orbital (GIAO) method at B3LYP/6311 + G(d,p) [43,44] in DMSO. The relative chemical shifts were obtained according to the general expression $\delta_{cald.} = \delta_{TMS}$-$\delta$, where δ_{TMS} shows the values of the corresponding tetramethylsilane (TMS) hydrogens shielding calculated at the same theoretical level.

2.7. In Vitro Cytotoxicity Testing

All the human cancer cells were purchased from American type cell collection (ATTC). LNCap (human prostate cancer) line were preserved in RPMI 1640 medium. LS174T (human colon carcinoma) and MCF-7 (breast cancer) cell lines were cultured in Dulbecco's modified Eagle's media and were supplemented with 10% fetal bovine serum, 2% penicillin/streptomycin. The cells were cultured at 37 °C in CO_2 incubator. The stock solution was prepared in DMSO. Shortly, the cells were seeded into 96-well plate for 24 h before treatment with various concentration (1, 5, 25, 50 and 100 μg/mL) of the compounds. After incubation for 24 h, the MTT cytotoxicity assay was performed as described previously in our studies [45]. The assay was performed using 1% DMSO as a vehicle control.

3. Results and Discussion

In this study, multi-dentate Schiff base (**L**) bearing coumarin unit and its Palladium(II) and Platinum(II) complexes have been obtained for the first time (Scheme 1). The structure of **L** and its metal complexes were evaluated by well-known spectroscopic technique (FT-IR, ^{1}H/^{13}C NMR and LC-MS), magnetic moment and molar conductivity studies (Supporting Information Figs. S1–4). The crystal structure and intermolecular interaction of **L** was clarified by X-ray diffraction method (Figs. 1, 2; Tables 1, 2 and Fig. S5, Table S1 in Supporting Information).

The metal complexes are stable at room condition in solid phase and their melting points are just over 250 °C. The lower molar conductivities of the complexes proves their non-electrolytic nature. As a result, metal complexes are supposed to have the general formula as $[ML_2]$, where M: Pt(II) and Pd(II).

3.1. Crystal Structure Analysis of L

The single crystal of **L** with dimensions 0.05 × 0.08 × 0.4 mm was obtained by slow evaporation of the solvent (EtOH). Single crystal data of **L** are exhibited in Table 1. ORTEP drawings with atomic numbers are given in Fig. 1. Fig. S5 shows the packing motif of **L** in supporting information. The plot correspond to thermal ellipsoids has the 50% probability level. Interactions via hydrogen bonding are summarized in Table 2. Selected bond lengths, bond and torsion angles of the Schiff base are given in Table S1 (See supporting information).

The molecule is stabilized by both intramolecular and intermolecular hydrogen bondings. The intramolecular bonding occurs between imine nitrogen and hydroxyl proton with a 1.870 Å distance and 148.6° angle. The intermolecular bonding occurs between double bonded oxygen of coumarin unit and proton attached to carbon of thiazole unit with a 2.571 Å distance and 143.20° angle. As expected, the coumarin moiety is nearly planar; the displacements of all ten atoms contained in the ring are < 0.022(16) Å from the least-squares plane. The thiazole ring is also planar and forms a torsion angle of 14.74° with the coumarin plane. The phenolic unit attached to the thiazole ring is twisted out of this ring plane with the torsion angle of 179.22°(1) for C8—N2—C9—C10 and makes a dihedral angle of 19.97° with the thiazole ring. The torsion angle between the phenol and the coumarin ring plane is 33.67. The C9—N2 [1.298(2) Å], C20—O3 [1.208(2) Å], C20—O2 [1.383(1) Å] and C19—O2 [1.379(2) Å] bond lengths are consistent with the double and single bond character expected in the imine and coumarin units [46–48]. A close C17—H10…O3 contact of 2.571(1) Å can be regarded as a strong intermolecular hydrogen bond. These contacts generate infinite chains along a-axis. The packing of the molecules exhibited layered stacking when viewed down the b-axis.

3.2. The Structural Characterization

3.2.1. Infrared Spectra

Infrared spectra of **L** (Supporting Information Fig. S1) and its complexes (Supporting Information Figs. S6 and S7) were recorded in KBr pellets. The selected frequencies belonging to functional groups were compared to find chelalation modes. The spectrum of ligand (**L**) exhibited sharp vibration band at 3417 cm^{-1} which belongs to phenolic ν(O—H). The vibration bands at 1738 cm^{-1}, 1589 cm^{-1}, 1235 cm^{-1} and 1150 cm^{-1} correspond to lactone ν(C═O), imine ν(C═N), phenolic ν(C—O), and lactone ν_{asym} (C—O—C) stretching vibrations were found, respectively. In complexes, imine vibration ν(C═N) was observed between 1535 and 1570 cm^{-1} which shows shifting to

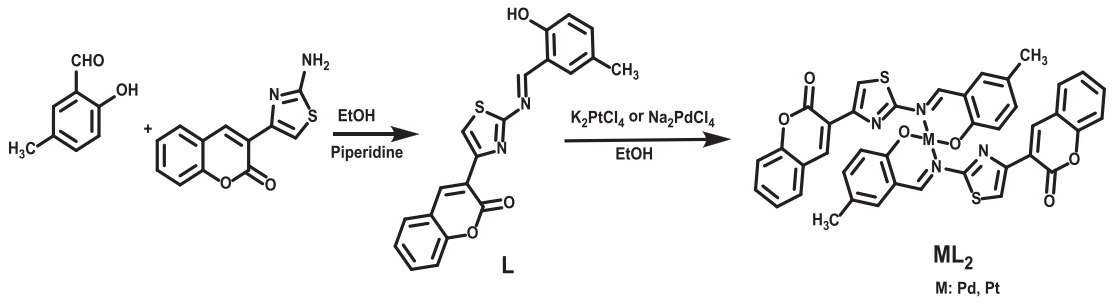

Scheme 1. Synthetic pathway of chemosensor **L** and its metal complexes.

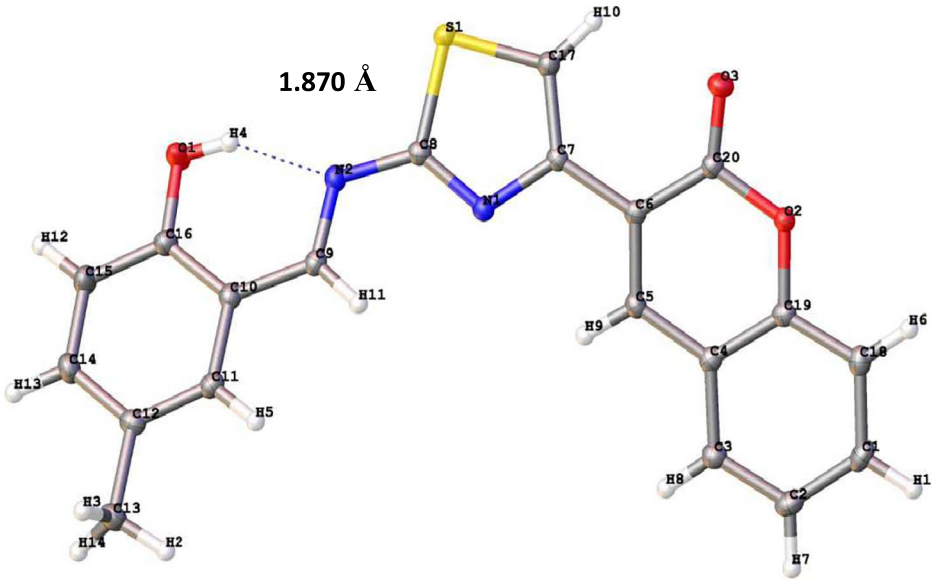

Fig. 1. ORTEP view of **L**, thermal ellipsoids are shown at the 50% probability level.

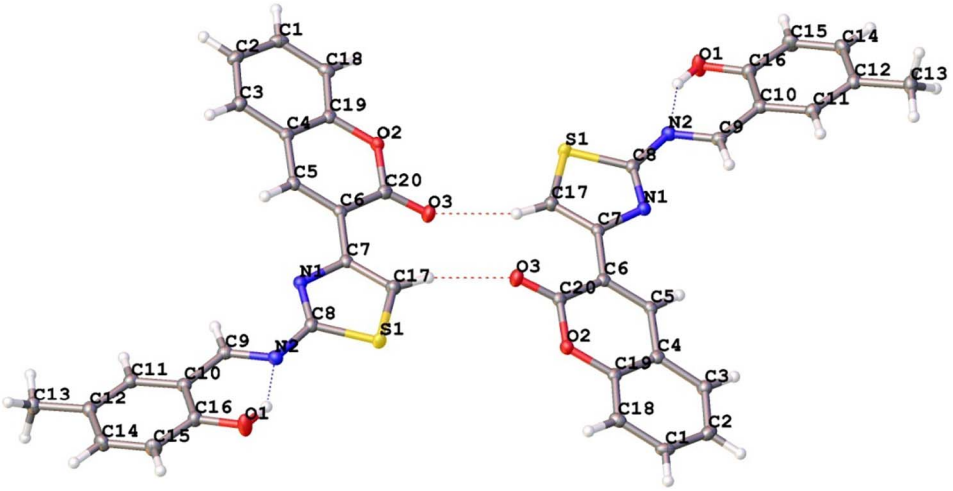

Fig. 2. Intermolecular hydrogen bonding of **L** is shown as a red dashed line. (For interpretation of the references to color in this figure legend, the reader is referred to the web version of this article.)

the lower frequencies by the coordination through imine-N (N → M) [49,50]. The ligands also display band at 1235 cm^{-1} which belongs to phenolic ν(C—O) vibrations. This frequency is strongly shifted to higher wave number (1249 cm^{-1} for Pd complex and 1258 cm^{-1} for Pt complex) by coordination through the phenolic-CO of the coumarin-thiazole Schiff base [51].

Coordination through oxygen and nitrogen atoms with metal ion is supported by the formation of new streching bands, (M—O) and ν(M—N) in the ranges 550–600 cm^{-1} and 450–530 cm^{-1}, respectively [49]. But, the vibration frequencies of ν(C═O) and ν_{asym}(C—O—C) belonging to the lactone ring in ligand (**L**) remain almost the same after chelation, thus it can be supposed that the lactone oxygen is not involved in chelation with the metal ion.

3.2.2. ^1H NMR Titration

$^1H/^{13}C$ NMR spectra of **L** were recorded in DMSO-d_6 using tetramethylsilane (TMS). ^1H NMR shifts were calculated by the gauge including atomic orbital (GIAO) method at B3LYP/6311 + G (d,p) [43,44] in DMSO. The experimental and calculated ^1H NMR shifts in DMSO-d_6 are listed in Table 3 and Fig. 3.

The **C**H_3 carbon on the phenol ring are easily distinguishable as a singlet, and they are observed at 2.28 ppm, and corresponding calculation value is 2.34 ppm. The phenyl protons (Hb, Hc, and Hd) are observed at 7.70, 7.30, and 6.93 ppm, and the corresponding calculation values are 7.55 ppm, 7.64 ppm, and 7.13 ppm, respectively. The thiazole proton (He, one H intensities) and coumarin ring proton (Hf) are distinguishable as a singlet, and they are observed at 8.35 ppm and 8.86 ppm, and the corresponding calculation values are 8.75 ppm and 9.24 ppm, respectively. The imine proton (Ha, one H intensities) is observed at 9.33 ppm which is attributed to the –C═N-H proton, and the corresponding calculation value is 9.93 ppm. Also OH proton is observed at 11.30 ppm and corresponding calculation value is 12.51 ppm.

In addition, the calculated ^1H NMR chemical shifts for **L** and **L-CN**$^-$ adduct, after nuclephilic addition process, are given in Table 3 with the corresponding experimental values, and also ^1H NMR spectra of **L** and **L-CN**$^-$ adduct after nuclephilic addition process are presented in Fig. 3. Since the experimental ^1H chemical shift values were not available for individual hydrogen, the average values for CH_3 hydrogen atoms are presented. Correlation coefficients of ^1H NMR were estimated as 0.945 for **L** and 0.985 for **L-CN**$^-$ from the linear correlations between calculated and experimental data of ^1H NMR. It is seen that, the theoretical results are in good agreement with the experimental values. The deviation between experimental and calculated values is 0.24 ppm for imine proton (**H**C = N) after the addition of CN^- to imine carbon.

Within the addition of CN^-, while the ligand signal began to shift to upper field and the intensities decreased, new signals began to appear (Fig. 3). Upon addition of 1 equiv. of CN^-, the imine (Ha) proton lost

Table 1
Crystal data and structure refinement parameters for **L**.

	L
Empirical formula	$C_{20}H_{14}N_2O_3S$
Formula weight	362.39
T(K)	100
λ(Å)	0.71073
Crystal system	Triclinic
Space group	P-1
Unit cell dimensions: (Å, °)	
a	7.9942(13)
b	8.8258(16)
c	13.186(2)
V(Å^3)	827.7(3)
α	73.202(7)
β	85.684(7)
γ	68.424(7)
Z	2
Absorption coefficient (mm^{-1})	0.219
Dcalc (g/cm^3)	1.454
F(000)	376
Crystal size (mm)	0.05 × 0.08 × 0.4
θ range for data collection (°)	2.59 to 27.45
Index ranges	−10 ≤ h ≤ 10 −11 ≤ k ≤ 11 −17 ≤ l ≤ 16
Reflections collected	29,181
Independent reflections	3772
Coverage of independent reflections (%)	99.7
Data/parameters	3772/239
Max. and min. transmission	0.989/0.9170
Final R indices [$I \geq 2\sigma(I)$]	R1 = 0.0332 w*R*2 = 0.0853
R indices (all data)	R1 = 0.0398 wR2 = 0.0903
Goodness-of-fit on F^2	1.036
Largest difference in peak and hole (e Å^{-3})	0.365/−0.230

Table 2
Hydrogen-bond geometry (Å, °) for **L**.

Donor–Hydrogen…Acceptor	D–H [Å]	H–A [Å]	D–A [Å]	D–H–A
O1—H4…N2	0.86	1.870	2.647	148.60°
C14—H3…O3	0.95	2.571	3.519	143.20°

Table 3
Comparison of calculated, experimental and after the addition of CN^- anion values of ^{1}H NMR chemical shifts (ppm) relative to TMS in DMSO for the **L**.

	^{1}H NMR			
Assign.	**L**		After the addition of CN^-	
	δ(exp.)	δ(calc.)[a]	δ(exp.)	δ(calc.)[a]
C**H**$_3$	2.28 (s,3H)	2.34	2.15 (s,3H)	2.23
C**H**$_{ar}$	6.93 (d, 1H) (Hd)	7.13		7.27
	7.30 (dd, 1H) (Hc)	7.64	6.47(d, 1H) (Hc)	6.72
	7.41 (t, 1H),	7.66	6.80(d, 1H) (Hd)	7.08
	7.47 (d, 1H),	7.65	7.01(s, 1H) (Hb)	7.66
	7.68 (dd, 1H)	7.91	7.40(m, 2H)	7.89
	7.70 (d, 1H) (Hb)	7.55	7.61(T, 1H)	8.06
	7.96 (dd, 1H)	8.06	7.88(d, 1H)	9.26
	8.35 (s, 1H) (He)	8.75		
	8.86 (s, 1H) (Hf)	9.24	8.67(s.1H) (Hf)	
HC=N	9,33 (s, 1H) (Ha)	9.93	5.69(Aliphatic) (Ha)	5.93
O**H**	11,30 (s, 1H)	12.51		12.64

and its intensity shifted slightly upperfield and new signal (Ha′) at 5.69 ppm appeared, which was expected with the addition of cyanide to imine carbon. Spectrum showed that, at the end of the titration, deprotonated **L** was also at present, even at low concentration. This result also supports the mechanisms of nucleophilic addition of cyanide at imine nitrogen and deprotonation mechanism of phenolic hydrogen and they occurred at the same time in NMR titration (Scheme 2) [35].

Also, to confirm this mechanism/assumption, proton NMR titrations were carried out with F^-, AcO^- and CN^- anions in DMSO-d_6 solution (Supporting Information Figs. S8 and S9). Addition of F^- and AcO^- anions caused the signals to shift upperfield, as expected, which is due to an overall change in the electron distribution in the conjugated system. By adding both 1 equiv. of F^- and AcO^- anions, the OH signal disappeared (Scheme 2). The titration continued till the addition of 4 equiv. of both anions (F- and AcO-), and the changes of the chemical shifts is given in Table 4.

In the ^{13}C NMR spectra for **L**: the **C**H3 carbon on the phenol ring, **C**=N carbon of **L**, phenolic HO-**C** carbon, **C**—O carbon of coumarin ring, and the **C**=O carbon of coumarin ring, were observed at 20.26 ppm, 164.53 ppm, 159.30 ppm, 158.71 ppm 167.88 ppm, respectively.

3.2.3. Mass Spectra

The electron impact mass spectrum of all synthesized compounds were recorded at 70 eV. LC–MS data of all compounds are presented in Table 5 and Figs S10, 11 (Supporting Information).

Mass spectra of **L** show the molecular ion peak, $[M + H]^+$ at *m/z* = 363.08 (%100) as the main peak, calc. mass for $C_{20}H_{14}N_2O_3S$ = 362.40 and the fragmentation peak corresponding to coumarin-thiazole ($C_{12}H_6O_2NS$) group at 245.03(%5), respectively. Molecular ion peak of metal complexes, $[M + NH4]^+$ and $[M + 2H]^+$ at *m/z* (intensity %), at 832 (10%) and 936 (5%) corresponding to $[PdL_2 + NH_4]^+$ and $[PtL_2 + 2H]^+$ were observed. PdL_2 gives mass fragments correspond to [PdL + H] at 469.30 (%30), $[PdL\text{-}2CO]^+$ at 406.01 (%100) as the main peak, respectively. PtL_2 gives fragments correspond to $[(PtL_2 + NH4)^-$ (Coumarin, $C_9H_5O_2$) $–C_2H_4]^+$ at 703.00 (%85), $[PtL\text{-}CH_3]^+$ at 541.14 (%5), $[L + 3H]^+$ at 366.00 (%9), $[CT]^+$ and at 245.03(%100) as the main peak, respectively.

3.2.4. Electronic Spectra and Magnetic Behavior

The electronic spectra of **L** and its M(II) complexes were studied in 10^{-3} M solutions and DMSO was used as the solvent. **L** has two bands at 350 nm and 386 nm which correspond to π → π* and n → π* transitions. In the electronic spectrum of the metal complexes, there are two electronic transition bands between 420 and 440 nm which correspond to the spin allowed $^1A_{1g} \rightarrow {}^1B_{1g}$ transition of square planar geometry. Pd(II) and Pt(II) complexes have electronic transition bands between 420 and 498 nm, which may be assigned to a square-planar geometry for metal complexes [35]. The room temperature magnetic moments for the two complexes, namely, $[PtL_2]$ and $[PdL_2]$ were measured and the values obtained were 0.10 B.M., 0.12 B.M., respectively. These values correspond to paired electron, suggesting diamagnetic character for the Pt(II) and Pd(II) complexes in square-planar geometry.

3.3. Anion Sensing Performance of L by UV–vis and Fluorimetric Titrations

As it's known, Schiff bases derived from aldehyde derivatives containing hydroxy group has tautomerization between phenol-imine and ketoamine forms due to the formation of O-H···N and O···H-N type hydrogen bonds. Chemosensor **L** has two absorption band at 350 nm and 386 nm as a result of the tautomerization.

The interaction of **L** with selected anions was investigated by using UV–vis and fluorescence spectroscopy. Anion titration studies were performed by adding standard volume of tetrabutylammonium (TBA) salt solutions of the various anions (F^-, Cl^-, Br^-, I^-, AcO^-, CN^-, $H_2PO_4^-$, HSO_4^-, and NO_3^-) to the solution of ligand (**L**) as shown in Fig. 4.

Absorption and emission maximum of **L** was observed at 345 nm and 510 nm in DMSO, respectively. While absorption band which was seen in 345 nm, decreased gradually upon addition of 14 equiv. of F^-, AcO^- and CN^-, to the solution of **L** and a new absorption band at

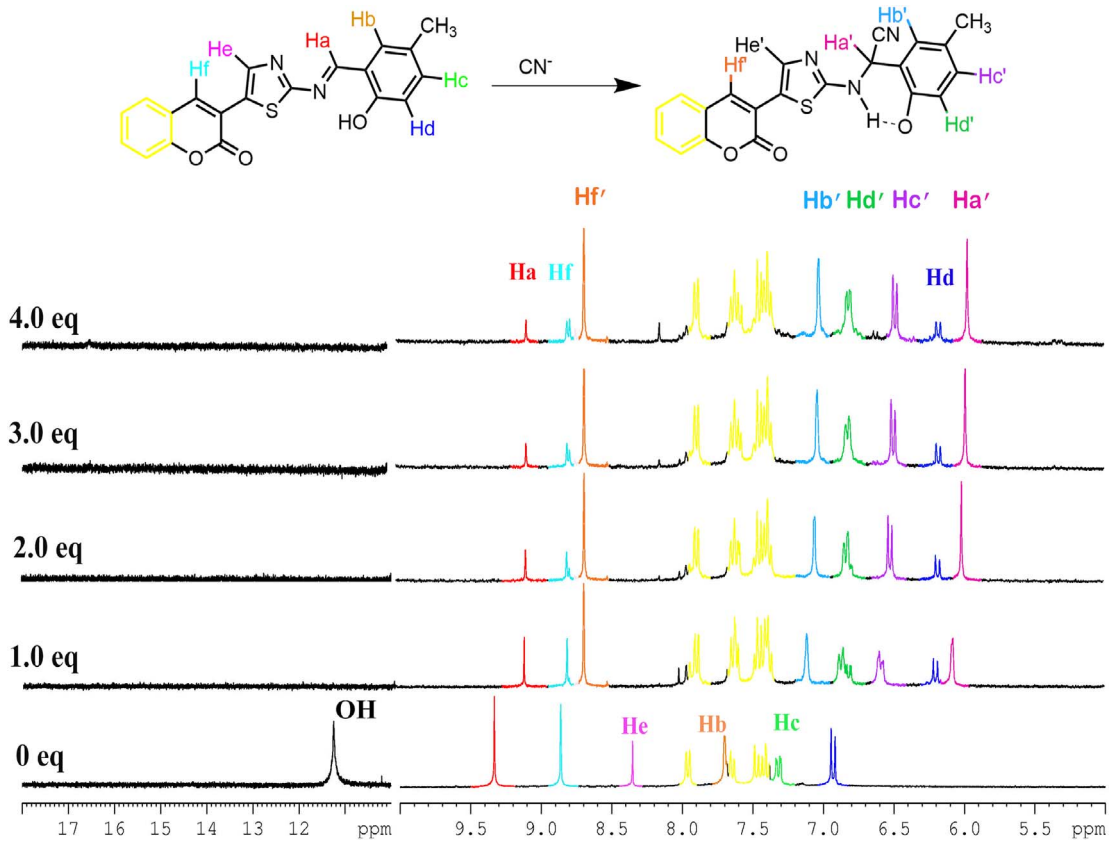

Fig. 3. Partial ^{1}H NMR (300 MHz) spectra obtained via titrations of **L** (1×10^{-2} M) with TBACN solution in DMSO-d_6.

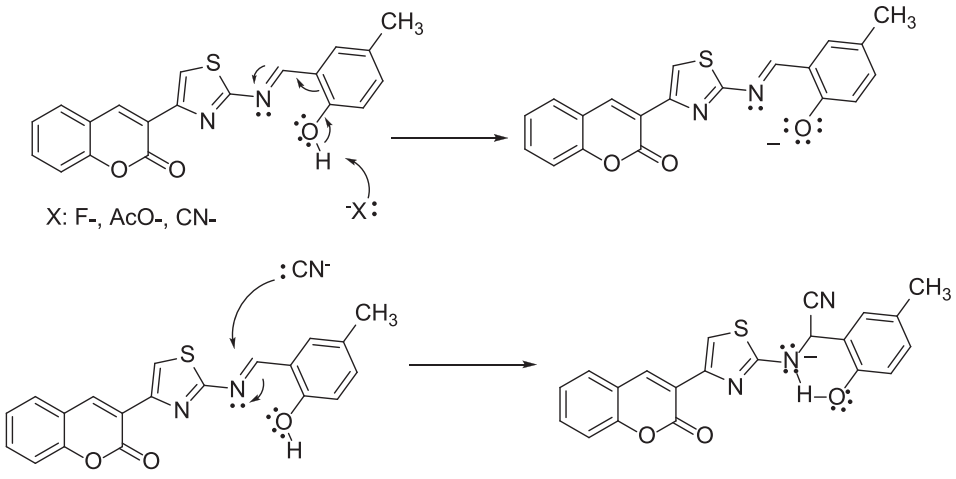

Scheme 2. A proposed binding mode of **L** in the presence of studied anions.

Table 4
Chemical shift values of chemosensor **L** and after adding 4 equiv. of F^- and OAc^- anions.

	L (in ppm)	L + TBAF	Δδ	L + TBAOAc	Δδ
Ha	9.33	9.05	+ 0.28	9.29	+ 0.04
Hb	7.70	7.35	+ 0.25	7.59	+ 0.11
Hc	7.30	6.46	+ 0.84	7.06	+ 0.24
Hd	6.93	6.13	+ 0.80	6.73	+ 0.20
He	8.35	7.98	+ 0.37	8.19	+ 0.16
Hf	8.86	8.79	+ 0.07	8.83	+ 0.03
CH_3	2.28	2.04	+ 0.24	2.18	+ 0.10

Table 5
The mass spectral data of Coumarine thiazole **L** and its complexes.

Compounds MW	Relative intensities of ligand and complexes (m/z, %) and assignment
L 362.40	$[M + H]^+$ (363.08%100), $[CT]^+$ (245.03, %5)
PdL_2 829.22	$[M + 2H]^+$ (833.00%10), $[PdL + H]^+$ (469.30, %30),$[PdL-2CO]^+$ (406.01, %100)
PtL_2 917.01	$[M + NH_4]^+$ (936.05, %5), $[(M + NH_4)\text{-Cou-}C_2H_4]^+$ (703.00, %85), $[PtL\text{-}CH3]^+$ (541.14, %5), $[L + 3H]^+$(366.00, %9), $[CT]^+$ (245.03, %100)

CT = Coumarin-thiazole.

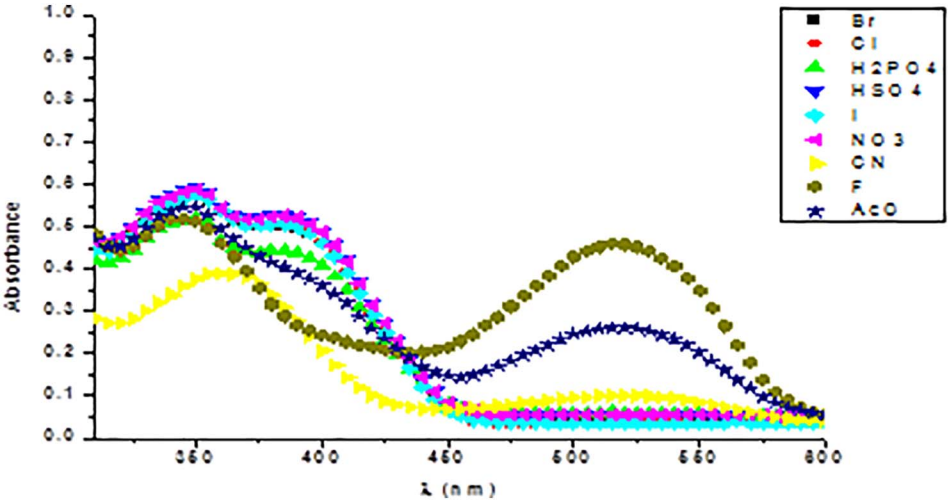

Fig. 4. Absorption spectra of probe **L** (3.0×10^{-5} M) upon addition of 1 equiv. of studied anions in DMSO.

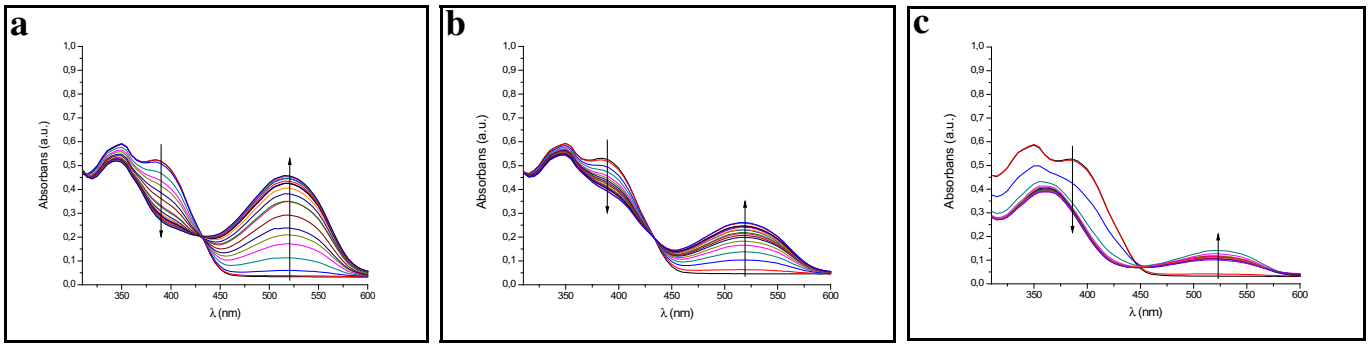

Fig. 5. UV–vis absorption spectral changes of **L** (3.0×10^{-5} M) upon addition of 14 equiv. of fluoride (a), acetate (b) and cyanide (c) anions in DMSO.

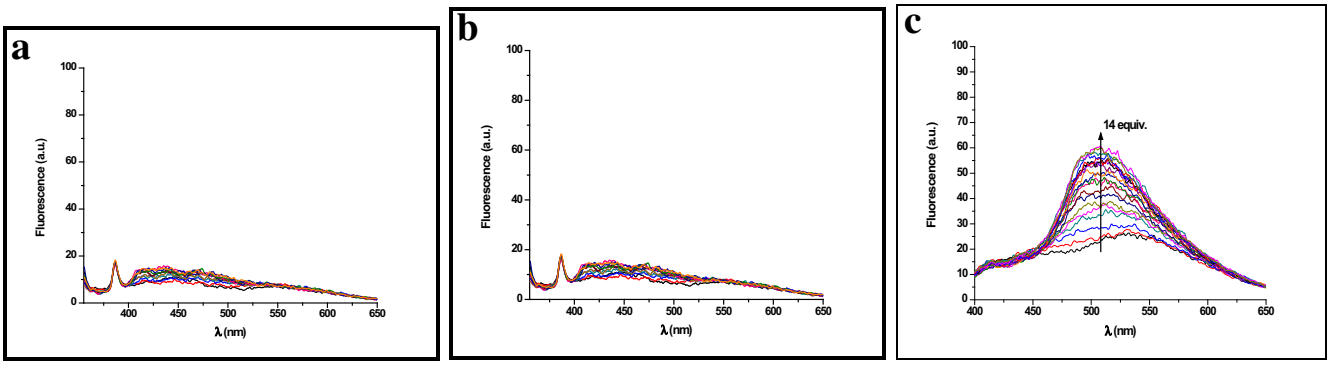

Fig. 6. Fluorescence spectra of **L** (1.0×10^{-5} M) upon addition of 14 equiv. of fluoride (a), acetate (b) and cyanide (c) anions in DMSO.

517 nm was created,

The observed bathochromic shift in UV–vis spectra, with addition of F^-, AcO^- and CN^- to receptor in DMSO, is due to ICT after deprotonation of the phenolic proton. In addition, the significantly enhanced fluorescent intensity was due to the addition of only CN^-. Cyanide has both basic and nucleophilic properties and has much weaker hydrogen bonding ability in comparison with F^- and AcO^-. Therefore, it was probably caused by the nucleophilic addition of CN^- to the imine functional group of **L** to afford a chemosensor **L**-CN adduct (Figs. 5, and 6). As expected, other anions such as Cl^-, Br^-, I^-, NO_3^-, HSO_4^- and $H_2PO_4^-$ did not cause any significant changes in their absorption and emission spectra.

Visual confirmation was also investigated by the real color photographs of solution of chemosensor **L** and upon addition of the anions (Fig. 7). Photos showed chemosensor **L** displayed a color change from light yellow to deep red upon addition of CN^-, whereas a light yellow-to-red color change was observed in the case of F^- and AcO^-. The result indicates that, chemosensor **L** can serve as a naked-eye indicator. More importantly under UV light, only addition of CN^- to chemosensor **L** gave an orange fluorescence. No significant color or emission changes were observed by the naked eye and under portable UV lamp, upon the addition of the other anions.

3.4. Theoretical Results

3.4.1. Theoretical Calculations for Determination of Sensing Mechanism Between L and Anions

In order to confirm the nucleophilic addition of CN^- to **L**, the geometrical optimizations and ^1H NMR chemical shifts were obtained. The optimized structures of **L**, **L**-F^-, **L**-AcO^- and **L**-CN^- are shown in

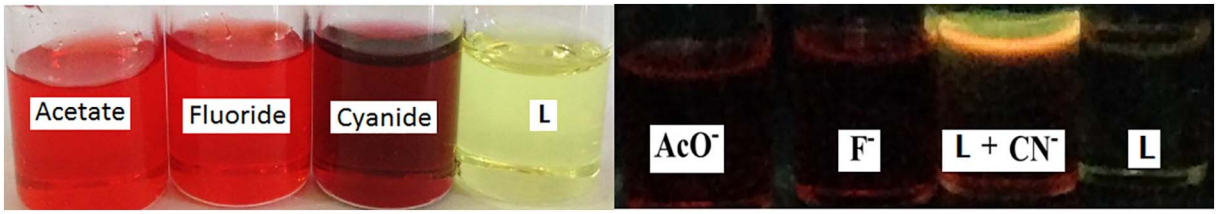

Fig. 7. Color changes of **L** (1.0×10^{-3} M in DMSO) under ambient light (left) and UV light (362 nm) (right) after addition of 1 equiv. of F^-, AcO^- and CN^-.

Fig. S12 (Supporting Information). For **L**, the dihedral angle of C17-C7-C6-C5 and C10-C9-N2-C8 is 180.0°, which indicates that **L** is completely planar. The atomic numbers are given in Fig. 2. As a result of this planarity, π-conjugation was provided and hence intermolecular charge transfer (ICT) occurs from the phenolic part to the thiazole moieties. There are only small changes in the dihedral values between the thiazole and phenolic moieties, as 3.46° and 4.63°, upon deprotonation of **L** with $\mathbf{F}^-$ and $\mathbf{AcO}^-$, respectively (Supporting Information Fig. 12 b and c). According to these small changes, as a red shift was observed in the absorption spectrum, it means that an ICT process exists. In other words, after the nucleophilic addition of $\mathbf{CN}^-$ to **L**, the planarity is distorted and the dihedral angles of C17-C7-C6-C5 and C10-C9-N2-C8 became 175.75° and − 160.89°, respectively. Due to the distortion of planarity, the π-conjugation between the phenolic and thiazole-coumarin moieties was not provided. As a result, there could be a blocking ICT process relative to **L**, which can be a reason for the changes in absorption and emission spectra.

3.4.2. Calculations for Pt (II) and Pd(II) Complexes

The optimized structure and FMOs (HOMO and LUMO) were illustrated in Fig. 8.

The highest occupied and lowest unoccupied molecular orbitals (FMOs:HOMO and LUMO) energy levels have importance on the determination of chemical reactivity of molecules [52–54] and the orbital density surfaces around the atoms indicate biologically active sites of the compounds. The lower LUMO energy and also lower energy gap ($\Delta E_{LUMO-HOMO}$) affect the binding activities of the molecules to DNA helix as receptor [55]. In general, the lower negative FMOs energies indicate that the prepared Schiff base and its complexes may be significant compounds for drug metabolism as oxidant and reductant. Dipole moment as well as the components of FMOs play an important role in biological activities. The decrease in dipole moment can be used to reasonably explain the rise of the biological activities of the compounds.

The obtained energy values of HOMO and LUMO levels, their energy band gaps ($\Delta E = E_{LUMO}\text{-}E_{HOMO}$), and the dipole moments (μ) are listed in Table 6. The calculated dipole moments of ligand and their complexes are $\mu_L = 6.2134$ D for L, $\mu_{[PdL2]} = 0.0154$ D for [PdL_2] complex and $\mu_{[PtL2]} = 0.0008$ D for [PtL_2] complex. Also, the FMOs energy gaps of ligand and complexes are $\Delta E = 3.402$ eV ($E_{LUMO} = -2.6142$ eV) for L, $\Delta E = 3.226$ eV ($E_{LUMO} = -2.0724$ eV) for [PdL_2] complex, and $\Delta E = 3.071$ eV ($E_{LUMO} = -2.0980$ eV) for [PtL_2] complex, respectively. The correlations between FMO and the dipole moment values with respect to anticancer activities show that, Pd(II) and Pt(II) complexes are more active than a free ligand. The FMOs have the highest orbital densities around phenolic unit and imine (C = N) part, which are responsible for biological activities of the molecules.

3.4.3. Molecular Electrostatic Potential Maps (MEPs)

The molecular electrostatic potential maps (MEPs) of **L** and its complexes are given in Fig. S13 (Supporting Information). The MEPs provide information about charge density distributions, chemically reactive sites and electrophilic interactions with biological systems [56,57]. The FMOs (HOMO and LUMO) and molecular electrostatic potentials maps (MEPs) are employed to understand the reactive sites which are responsible for biological activities. The positive electrostatic potential surfaces, colored in blue, refer to repulsion of the proton by atomic nuclei in the lower electron density regions. The negative regions colored in shades of red are regarded as nucleophilic sites whereas positive regions (in blue color) as electrophilic centers [58–61]. The MEP analysis of our compounds reveals that, negative potentials (red regions) are concentrated on O atom of phenolic group and also lactone sites moieties. The oxygen atom on phenol ring is supposed as most active sites to interact with biological molecules.

3.5. In Vitro Antitumor Activity

There are a lot of reports about cytotoxicity levels depending on the structural differences of the platinum complexes [62,63]. The different cytotoxicity levels depend on the molecular structure and cell lines. It has been observed that, metal complexes interact with DNA helix by noncovalent intercalation, groove or outer electrostatic binding [21]. The metal complexes are bounded to DNA helix by a series of weak π-stacking interactions between the base pairs (intercalation), hydrogen bonding and van der Waals interactions [64].

It is well known that, the palladium complexes were selected due to their structural and thermodynamic similarities with Platinum complexes, as well as being cost effective. These make Pd(II) complexes the preferred compounds in search of new potential anti-cancer drugs. However, Pd(II) derivatives generally show higher toxicity and lower anti-cancer activity because of the lability, which enhances quick access to biological target and rapid interference with essential biochemical processes. Up to now, many mono-, di-, or polynuclear palladium(II) complexes with various N- or S-donor combinations have been evaluated as chemotherapeutic agents for cancer therapy. It was reported that *cis/trans*-Pd(II) complexes of aromatic N-donor molecules as ligand were more active than *cis/trans*-Pt(II) complexes [65,66]. However, the most of the *trans*-palladium complexes showed better activities than other *cis*-platin, and also *cis*-palladium isomers. It is interesting that these palladium complexes showed activities equal to (or higher than) *cis*-platin, carboplatin and oxaliplatin, in vitro, and these results are in a disagreement with the previous studies that *cis*-isomers are more effective than the *trans*-ones [67].

In this respect, we synthesized Pt(II) and Pd(II) complexes containing N,S donors in thiazole rings. The anti-cancer activity results showed that, *trans*-Pd(II) complexes are more active than the *trans*-Pt (II) complexes against breast adenocarcinoma (MCF-7), human prostate adenocarcinoma (LNCAP) and human colon carcinoma (LS174T) cell lines. It has been reported, generally, coumarin derivatives are reduced due to the cell viability against different cell lines [68,69]. Beside these, the structure activities of coumarins were reported, and according to the results, anticancer activities of these compounds are both structure and dose-dependent [70]. The percentage cell viability of the synthesized compounds decreases as a function of increasing concentration in IC_{50} values in μg/mL. At 50 μM concentrations of Pd(II)/Pt(II) complexes, significant decrease in percentage viability of cell lines. The most effective dose is found to be 100 μM for both the synthesized ligand and its complexes (Fig. 9a, b and c).

The half maximal inhibitory concentration (IC_{50}) represents the

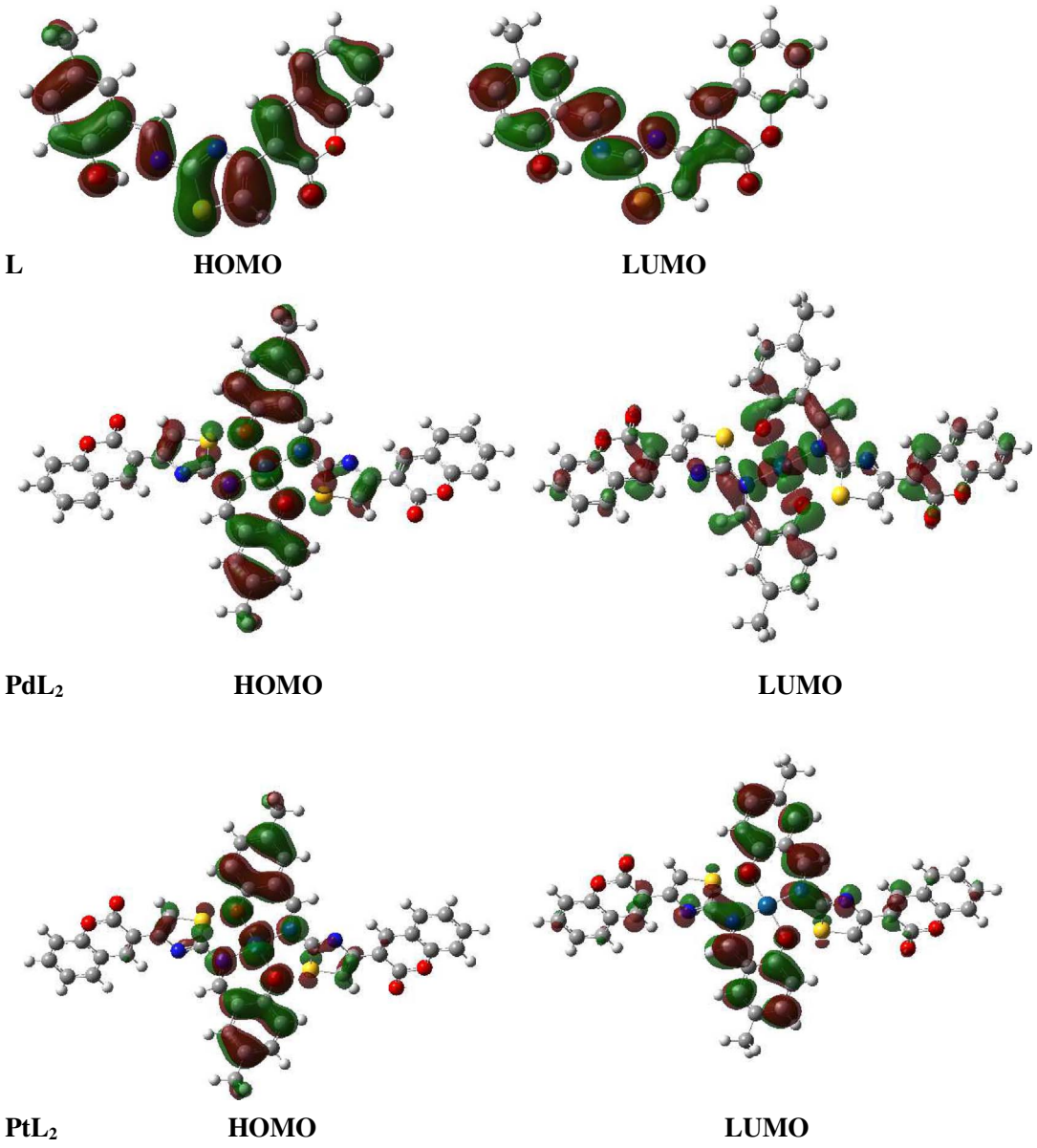

Fig. 8. The optimized structures and molecular orbitals of **L** and its complexes (PtL_2, PdL_2).

Table 6
MO energies, energy band gaps and Dipol Moment of the **L** and its complexes.

Compounds	E_{HOMO} (eV)	E_{LUMO} (eV)	ΔE (eV)	μ(D)
L	− 6.0166	− 2.6142	3.402	6.2134
[PdL_2]	− 5.2983	− 2.0724	3.226	0.0154
[PtL_2]	− 5.1693	− 2.0980	3.071	0.0008

concentration of the tested agent that is required for 50% inhibition of the tumor cell viability. The inhibition concentration results in IC_{50} values (in μg/mL) are presented in Table 7.

The IC_{50} values of the two metal complexes are lower than that of **L** (except for the activity of the Pt(II) complex against human colon carcinoma, LS174T cell line) in the tested tumor cell lines, which suggests that chelated transition metal ions play an important role in higher activities of the complexes. It is evident that, the Pd(II) complex demonstrated better growth-inhibiting effect than the Pt(II) complex against MCF-7, LNCAP, and LS174T cells under the experimental conditions used herein. According to the results of viability of LS174T cells, at concentration of 50 μM and 100 μM of the ligand (IC_{50} μg/mL = 54.42) and PdL_2 complex (IC_{50} μg/mL = 15.98) caused decreasing effect on cell viability, while PtL_2 complex (IC_{50} μg/ml > 100) showed no effect. In addition, Pd(II) complex exhibited good activity against MCF-7 cell lines (IC_{50} = 18.15 μg/mL). Finally, Pd(II) complex had the most prominent activity against LNCaP cell lines (IC_{50} = 10.05 μg/mL) compared to other compounds.

4. Conclusions

Schiff base based chemosensor (**L**) and Pt(II)/Pd(II) complexes were synthesized and their structures were determined by several spectroscopic methods, magnetic moment and molar conductivity measurements. The structure of **L** was also clarified by X-ray spectroscopy. All the experimental analysis results show that, **L** acts as a bidentate ligand chelating through imine nitrogen and phenolic oxygen sites. In the light of spectroscopic methods, the supposed structures of the metal complexes are given in Scheme 1. The anion selectivity and sensitivity potential of chemosensor were investigated by fluorescence, absorption and ^{1}H NMR titration methods. DFT method was used to explain the obtained experimental results. The results showed that, **L** can be

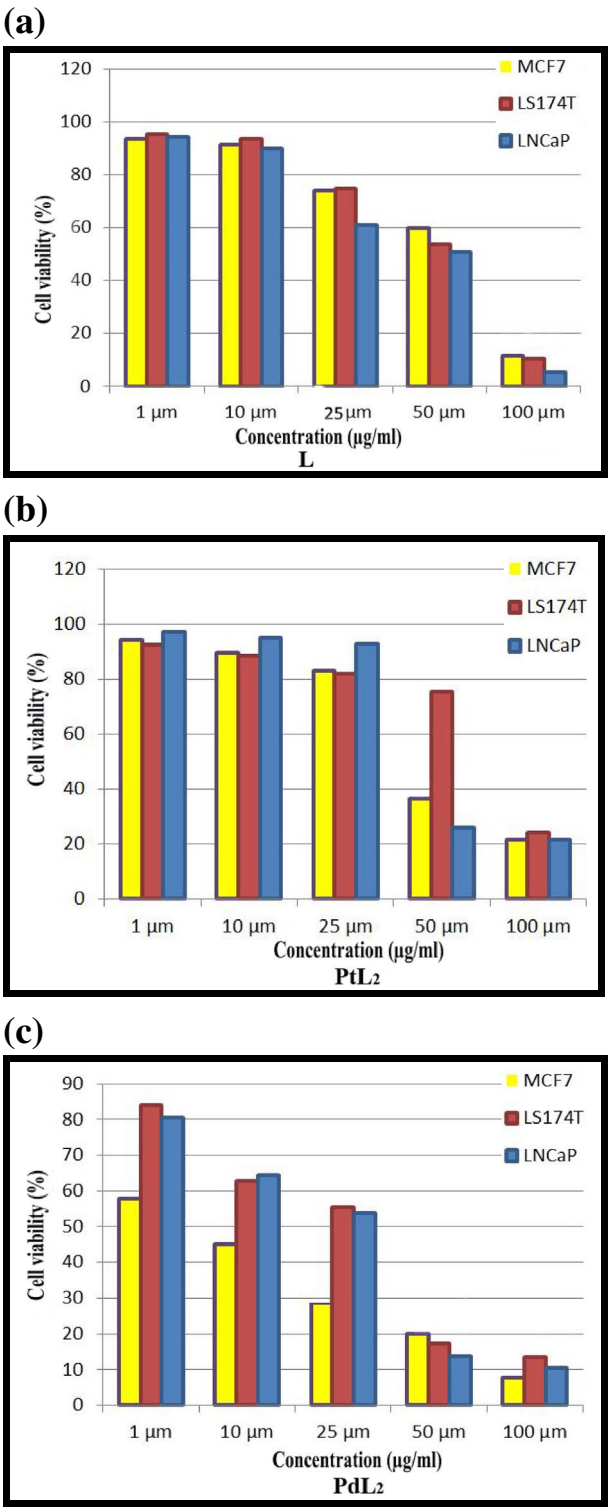

Fig. 9. Evaluation of cytotoxicity against MCF-7, LS174T and LNCaP cell lines of **L** (a), PtL_2 complex (b) and PdL_2 complex (c).

utilized to simultaneously analyse F^-, AcO^- and CN^- ions by two new detection modes and **L** has higher selectivity towards CN^- anion than F^- and AcO^- anions. The interaction of CN^- with **L** increased the fluorescence emission and provided a *turn on* response. Thus, **L** can be applied as probe for detection of CN- via light-up. On the other hand, anti-cancer activities of **L** and its metal complexes were determined in vitro using MTT assay on MCF-7, LS174T and LNCAP human cancer lines. The anti-tumor activity results show that, the Schiff base metal

Table 7
In vitro antitumor activities of **L** and its metal complexes against three human cancer cell lines for 24 h.

Compounds	MCF-7 IC_{50} µg/ml	LNCaP IC_{50} µg/ml	LS174T IC_{50} µg/ml
L	57.29	48.65	54.42
PtL_2	33.97	21.53	> 100
PdL_2	18.15	10.05	15.98

complexes have good cytotoxicity effects on the human cell lines. In our study, it was found that palladium complexes have better activities with lower IC_{50} values (10.05–18.15 µg/mL) than the platinum complexes with higher IC_{50} values (21.53 − . > 100 µg/mL). The computed electronic descriptors support the higher activity trend of metal(II) complexes, especially Pd(II) complex than the ligand.

Acknowledgements

We thank TUBITAK [Project Grant No: 214Z152] for financial support. We are also thankful to ITU for the use of the Bruker SMART BREEZE CCD diffractometer (purchased under grant No.2010K120480 of the State of Planning Organization).

Appendix A. Supplementary data

Supplementary data (Original FTIR, ^1H NMR, ^{13}C NMR, LCMS and x-ray spectra, figures, tables, optimized structures and the molecular electrostatic potential map belong to chemosensor (**L**) and its complexes can be found.) associated with this article can be found in the online version, at: https://doi.org/10.1016/j.jphotobiol.2017.11.030

References

[1] B. Rajitha, K.V. Naveen, P. Someshwar, M.J. Venu, R.P. Narsimha, R.Y. Thirupathi, Dipyridine copper chloride catalyzed coumarin synthesis via pechmann condensation under conventional heating and microwave irradiation, ARKIVOC xii (2006) 23–27.
[2] R. O'Kennedy, R.D. Thornes, Coumarins: Biology Application and Mode of Action, JohnWiley and Sons, New York, 1997, p. 348.
[3] M. Zabradnic, The Production and Application of Fluorescent Brightening Agents, John wiley and sons, New york, 1992.
[4] M. Maeda, Laser Dyes, Academic, New York, 1994.
[5] B. Nikhil, B. Shikha, P. Anil, N.B. Prakash, Diverse pharmacological activities of 3-substituted coumarins: a review, Int. Res. J. Pharm. 3 (2012) 24–29.
[6] S. Venkataraman, R. Meera, V. Ramachandran, P. Devi, A. Aruna, S.P.T. Parameswari, K. Nagarajan, Antioxidant and anticoagulant activity of novel n-substituted-4- methyl-5,7-dihydroxyl coumarin and its ester derivatives, Int J. Pharm. Rev & Res. 4 (2014) 25–32.
[7] U.S. Weber, B. Steffen, C.P. Siegers, Antitumour-activities of coumarin, 7-hydroxycoumarin and its glucuronide in several human tumor cell lines, Res. Commun. Mol. Pathol. Pharmacol. 99 (1998) 193–206.
[8] D. Cooke, Studies on the Mode of Action of Coumarins (Coumarin,6-hydroxycoumarin, 7-hydroxycoumarin and Esculetin) at a Cellular Level (PhD Thesis), Dublin City University, Dublin, Ireland, 1999.
[9] D. Egan, P. James, D. Cooke, R. O'Kennedy, Studies on the cytostatic and cytotoxic effects and mode of action of 8-nitro-7Hydroxycoumarin, Cancer Lett. 118 (1997) 201–211.
[10] D. Cooke, R. O'Kennedy, Comparison of the tetrazolium salt assay for succinate dehydrogenase with the cytosensor microphysiometer in the assessment of compound toxicities, Anal. Biochem. 274 (1999) 188–194.
[11] E. Budzisz, E. Brzezinska, U. Krajewska, M. Rozalski, Cytotoxic effects, alkylating properties and molecular modelling of Coumarin derivatives and their phosphonic analogues, Eur. J. Med.Chem. 38 (2003) 597–603.
[12] M. Raghu, A. Nagaraj, R.Ch Sanjeeva, Synthesis and *in vitro* study of novel bis-[3-(2-arylmethylidenimino-1,3-thiazol-4-yl)-4-hydroxy-*2H*-chromen-2-one-6-yl] methane and bis-[3-(2-arylidenhydrazo-1,3-thiazol-4-yl)-4-hydroxy-*2H*-chromen-2-one-6-yl] methane as potential antimicrobial agents, J. Heterocycl. Chem. 46 (2009) 261–267.
[13] A. Gursoy, N. Karali, Synthesis, characterization and primary antituberculosis activity evaluation of 4-(3coumarinyl)-3-benzyl-4-thiazolin-2-one benzylidene hydrazones, Turk. J. Chem. 27 (2003) 545–551.
[14] F. Chimenti, B. Bizzarri, A. Bolasco, D. Secci, P. Chimenti, A. Granese, S. Carradori, M. D'Ascenzio, D. Lilli, D. Rivanera, Synthesis and biological evaluation of novel 2,4disubstituted-1,3-thiazoles as anti-Candida spp. agents, Eur. J. Med. Chem. 46

(1) (2011) 378–382.
[15] A. Kamal, S. Adil, J. Tamboli, B. Siddardha, U. Murthy, Synthesis of coumarin linked naphthalimide conjugates as potential anticancer and antimicrobial agents, Lett. Drug Des. Discovery 6 (2009) 201–209.
[16] R.G. Kalkhambkar, G.M. Kulkarni, H. Shivkumar, R.N. Rao, Synthesis of novel triheterocyclicthiazoles as antiinflammatory and analgesic agents, Eur. J. Med. Chem. 42 (10) (2007) 1272–1276.
[17] B.Z. Kurt, I. Gazioglu, F. Sonmez, M. Kucukislamoglu, Synthesis, antioxidant and anticholinesterase activities of novel coumarylthiazole derivatives, Bioorg. Chem. 59 (2015) 80–90.
[18] J.T. Desai, C.K. Desai, K.R. Desai, A convenient, rapid and eco-friendly synthesis of isoxazoline, heterocyclic moiety containing bridge at 2`-amine as potential pharmacological agent, J. Iran. Chem. Soc. 5 (2008) 67–73.
[19] B. Naik, K.R. Desai, Novel approach for rapid and efficient synthesis of heterocyclic Schiff bases and azetidinones under microwave irradiation, Indian J. Chem. 45 (B) (2006) 267–271.
[20] N. Siddiqui, M.F. Arshad, S.A. Khan, Synthesis of some new coumarin incorporated thiazolyl semicarbazones as anticonvulsants, Acta Pol. Pharm. Drug Res. 66 (2009) 161–167.
[21] A.S. Abu-Surrah, H. Haitham, Y.M. Al-Sa'doni, Abdalla, Palladium-based chemotherapeutic agents: routes toward complexes with good antitumor activity, Cancer Ther. 6 (2008) 1–10.
[22] M. Manjunatha, H.V. Naik, Ajaykumar D. Kulkarni, A.P. Sangamesh, DNA cleavage, antimicrobial, anti-inflammatory anthelmintic activities, and spectroscopic studies of Co(II), Ni(II), and Cu(II) complexes of biologically potential coumarin Schiff bases, J. Coord. Chem. 64 (24) (2011) 4264–4275.
[23] P.P. Hankare, S.R. Naravane, V.M. Bhuse, S.D. Delekar, A.H. Jagtap, Synthesis and characterization of Mn(II), Co(II), Ni(II), Cu(II) and Zn (II) azo coumarin complexes, Indian J. Chem. 43 (7) (2004) 1464–1467.
[24] B.C. Raju, J.M. Wells, G. Nyland, R.H. Brylansky, S.K. Lowe, Plum leaf scald: isolation, culture, and pathogenicity of the causal agent, Phytopathology 72 (1982) 1460–1466.
[25] E. Wong, M. Christen Giandomenico, Current status of platinum-based antitumor drugs, Chem. Rev. 99 (1999) 2451–2466.
[26] A.M. Florea, D. Büsselberg, Cisplatin as an anti-tumor drug: cellular mechanisms of activity, drug resistance and induced side effects, review, Cancer 3 (2011) 1351–1371.
[27] G. Natile, M. Coluccia, Current status of trans-platinum compounds in cancer therapy, Coord. Chem. Rev. 216–217 (2001) 383–410.
[28] T. Boulikas, M. Vougiouka, Cisplatin and platinum drugs at the molecular level, Oncol. Rep. 10 (2003) 1663–1682.
[29] M.J. Cleare, J.D. Hoeschele, Studies on the antitumor activity of group VIII transition metal complexes. Part I. Platinum(II) complexes, Bioinorg. Chem. 2 (1973) 187–210.
[30] S.M. Sbovata, F. Bettio, M. Mozzon, R. Bertani, A. Venzo, F.B. Rino, A. Michelin, V. Gandin, C. Marzano, Cisplatinum and transplatinum complexes with benzyliminoether ligands; synthesis, characterization, structure-activity relationships, and in vitro and in vivo antitumor efficacy, J. Med. Chem. 50 (2007) 4775–4784.
[31] F.V. Rocha, C.V. Barra, A.V.G. Netto, A.E. Mauro, I.Z. Carlos, R.C.G. Frema, S.R. Ananias, M.B. Quilles, A. Stevanato, M.C. da Rocha, 3,5-Dimethyl-1-thiocarbamoylpyrazole and its Pd(II) complexes: Synthesis, spectral studies and antitumor activity, Eur. J. Med. Chem. 45 (2010) 1698–1702.
[32] E. Ulukaya, F. Ari, K. Dimas, E.I. Ikitimur, E. Guney, V.T. Yilmaz, Anti-cancer activity of a novel palladium(II) complex on human breast cancer cells in vitro and in vivo, Eur. J. Med. Chem. 46 (10) (2011) 4957–4963.
[33] T. Rau, R. Van Eldik, A. Sigel, H. Sigel (Eds.), Metal Ions in Biological Systems, vol. 31, Marcel Dekker, New York, 1996, pp. 339–378.
[34] T.N. Gligorijevi, T.T. Todorovi, T.S. Radulovi, T.D. Sladi, T.N. Filipovi, D. Godevac, T.D. Jeremi, T.K. Andelkovi, Synthesis and characterization of new Pt(II) and Pd(II) complexes with 2quinoline carboxaldehyde selenosemicarbazone: cytotoxic activity evaluation of Cd(II), Zn(II), Ni(II), Pt(II) and Pd(II) complexes with heteroaromatic seleno semi carbazones, Eur. J. Med. Chem. 44 (2009) 1623–1629.
[35] Ö. Şahin, Ü. Özmen Özdemir, N. Seferoğlu, B. Aydıner, M. Sarı, T. Tunç, Z. Seferoğlu, A highly selective and sensitive chemosensor derived coumarin-thiazole for colorimetric and fluorimetric detection of CN- ion in DMSO and aqueous solution: synthesis, sensing ability, Pd(II) /Pt(II) complexes and theoretical studies, Tetrahedron 72 (2016) 5843–5852.
[36] F. Denizot, R. Lang, Rapid, Colorimetric assay for cell growth and survival: modifications to the tetrazolium dye procedure giving improved sensitivity and reliability, J. Immunol. Methods 89 (1986) 271–277.
[37] G.M. Sheldrick, SHELXS-97, Program for Crystal Structure Solution, University of Göttingen, 1997.
[38] G.M. Sheldrick, A short history of SHELX, Acta Crystallogr. A 64 (2008) 112–122.
[39] O.V. Dolomanov, L.J. Bourhis, R.J. Gildea, J.A.K. Howard, H. Puschmann, OLEX2: a complete structure solution, refinement and analysis program, J. Appl. Crystallogr. 42 (2009) 339–341.
[40] M.J. Frisch, G.W. Trucks, H.B. Schlegel, G.E. Scuseria, M.A. Robb, J.R. Cheeseman, G. Scalmani, V. Barone, B. Mennucci, G.A. Petersson, H. Nakatsuji, M. Caricato, X. Li, H.P. Hratchian, A.F. Izmaylov, J. Bloino, G. Zheng, J.L. Sonnenberg, M. Hada, M. Ehara, K. Toyota, R. Fukuda, J. Hasegawa, M. Ishida, T. Nakajima, Y. Honda, O. Kitao, H. Nakai, T. Vreven, Jr. Montgomery, J.E. Peralta, F. Ogliaro, M. Bearpark, J.J. Heyd, E. Brothers, K.N. Kudin, V.N. Staroverov, R. Kobayashi, J. Normand, K. Raghavachari, A. Rendell, J.C. Burant, S.S. Iyengar, J. Tomasi, M. Cossi, N. Rega, J.M. Millam, M. Klene, J.E. Knox, J.B. Cross, V. Bakken, C. Adamo, J. Jaramillo, R. Gomperts, R.E. Stratmann, O. Yazyev, A.J. Austin, R. Cammi, C. Pomelli, J.W. Ochterski, R.L. Martin, K. Morokuma, V.G. Zakrzewski, G.A. Voth, P. Salvador, J.J. Dannenberg, S. Dapprich, A.D. Daniels, O. Farkas, J.B. Foresman, J.V. Ortiz, J. Cioslowski, D.J. Fox, Gaussian 09, Revision C.01, Gaussian, Wallingford, CT, 2009.
[41] A.D. Becke, Density functional thermochemistry. III. The role of exact exchange, J. Chem. Phys. 98 (1993) 5648–5652.
[42] C. Lee, W. Yang, R.G. Parr, Development of the Colle-Salvetti correlation-energy formula into a functional of the electron density, Phys. Rev. B 37 (1998) 785–789.
[43] R. Dichfield, An international journal at the Interface between chemistry and physics, Mol. Phys. 27 (1974) 789.
[44] K. Wolinski, J.F. Hinton, P. Pulay, Efficient implementation of the gauge-independent atomic orbital method for NMR chemical shift calculations, J. Am. Chem. Soc. 112 (1990) 8251.
[45] U. Özdemir Özmen, F. İlbiz, A. Balaban Gündüzalp, N. Özbek, Z. Karagöz Genc, F. Hamurcu, S. Tekin, Alkyl sulfonic acide hydrazides: synthesis, characterization, computational studies and anticancer, antibacterial, anticarbonic anhydrase II (hCA II) activities, J. Mol. Struct. 1100 (2015) 464–474.
[46] D.S. Reddy, K.M. Hosamani, H.C. Devarajegowda, M.M. Kurjogi, A facile synthesis and evaluation of new biomolecule-based coumarin–thiazoline hybrids as potent anti-tubercular agents with cytotoxicity, DNA cleavage and X-ray, RSC Adv. 5 (2015) 64566–64581.
[47] A. Arshad, H. Osman, C.K. Lam, M. Hemamalini, H.-K. Fun, (*E*)-3-(2-{2-[1-(3-Hydroxyphenyl) ethylidene]hydrazinyl}-1,3-thiazol-4-yl)-2*H*-chromen-2-one, Acta Crystallogr. Sect. E: Struct. Rep. Online 67 (2011) 1072–1073.
[48] A. Arshad, H. Osman, C.K. Lam, C.K. Quah, H.K. Fun, 3-{2-[2-(2-Fluorobenzylidene)hydrazinyl]-1,3-thiazol-4-yl}-2*H*-chromen-2-one, Acta Crystallogr. Sect. E: Struct. Rep. Online 66 (2010) 1446–1447.
[49] U.O. Ozdemir, N. Akkaya, N. Ozbek, New Ni(II), Pd(II), Pt(II) complexes with Aromatic methanesulfonylhydrazone based ligands. Synthesis, spectroscopic characterization and in vitro antibacterial evaluation, Inorg. Chim. Acta 400 (2013) 13–19.
[50] S. Sert, O.S. Senturk, U. Ozdemir, N. Karacan, F. Ugur, Synthesis and characterization of the products from reaction of metal carbonyls [M(CO)(6) (M = Cr, Mo, W), Re(CO)(5)Br, Mn(CO)(3)Cp] with salicylaldehydemethanesulfonyl hydrazone, J. Coord. Chem. 57 (3) (2004) 183–188.
[51] O.S. Senturk, U. Ozdemir, S. Sert, N. Karacan, F. Ugur, Photochemical reactions of metal carbonyls [M(CO)(6) (M = Cr, Mo, W), Re(CO)(5)Br, Mn(CO)(3)Cp] with salicylaldehyde ethanesulfonylhydrazone, J. Coord. Chem. 60 (2) (2007) 229–235.
[52] U. Ozdemir Ozmen, A. Altuntas, A.B. Gunduzalp, F. Arslan, F. Hamurcu, New Aromatic/heteroaromatic propanesulfonylhydrazone compounds: Synthesis, physical properties and inhibition studies against carbonic anhydrase II (CAII) enzyme, Spectrochim. Acta A 128 (2014) 452–460.
[53] A.B. Gündüzalp, G. Parlakgümüs, D. Uzun, U.O. Ozmen, N.T. Tunç, Carbonic anhydrase inhibitors: synthesis, characterization and inhibition activities of furan sulfonylhydrazones against carbonic anhydrase I (hCA I), J. Mol. Struct. 1105 (2016) 332–340.
[54] U.O. Ozdemir, E. Aktan, F. Ilbiz, A.B. Gündüzalp, N. Ozbek, M. Sarı, Ö. Çelik, S. Saydam, Characterization, antibacterial, anticarbonic anhydrase II isoenzyme, anticancer, electrochemical and computational studies of sulfonic acide hydrazide derivative and its Cu(II) complex, Inorg. Chim. Acta 423 (2014) 194–203.
[55] A. Balaban Gündüzalp, U. Ozdemir Ozmen, B.S. Çevrimli, S. Mamas, S. Çete, Synthesis, characterization, electrochemical behavior and antimicrobial activity of aromatic/heteroaromatic sulfonylhydrazone derivatives, Med. Chem. Res. 23 (2014) 3255–3268.
[56] S. Chidangil, M.K. Shukla, P.C. Mishra, A molecular electrostatic potential mapping study of some fluoroquinolone anti-bacterial agents, J. Mol. Model. 4 (1998) 250–258.
[57] P. Ekmekcioglu, N. Karabocek, S. Karabocek, M. Emirik, Synthesis, structural and biochemical activity studies of a new hexadentate Schiff base ligand and its cu(II), Ni(II), and co(II) complexes, J. Mol. Struct. 1099 (2015) 189–196.
[58] F.J. Luque, J.M. Lopez, M. Orosco, Perspective on Electrostatic interactions of a solute with a continuum. A direct utilization of ab initio molecular potentials for the prevision of solvent effects, Theor. Chem. Accounts 103 (2000) 343–345.
[59] E. Aktan, B. Babür, Z. Seferoğlu, T. Hökelek, E. Şahin, Synthesis and structure of a novel hetarylazoindole dye studied by X-ray diffraction, FT-IR, FT-Raman, UV-vis, NMR spectra and DFT calculations, J. Mol. Struct. 1002 (2011) 113–120.
[60] B. Babür, N. Seferoğlu, E. Aktan, T. Hökelek, E. Şahin, Z. Seferoğlu, Phenylazoindole dyes 3: determination of azo-hydrazone tautomers of new phenylazoindole dyes in solution and solid state, J. Mol. Struct. 1081 (2015) 175–181.
[61] E. Scrocco, J. Tomasi, Electronic molecular structure, reactivity and intermolecular forces: an euristic interpretation by means of electrostatic molecular potentials, J. Adv. Quantum. Chem. 11 (1978) 115–121.
[62] J. Mier-Vinue, J. Lorenzo, A.M. Montana, V. Moreno, F.X. Aviles, Synthesis, DNA interaction and cytotoxicity studies of cis{[1,2bis(aminomethyl)cyclohexane]dihalo} platinum(II) complexes, J. Inorg. Biochem. 102 (2008) 973–987.
[63] V. Vo, Z.G. Kabuloglu-Karayusuf, S.W. Carper, B.L. Bennett, C. Evilia Novel, 4, 4-diether-2, 2-bipyridine cisplatin analogues are more efective than cisplatin at inducing apoptosis in cancer cell lines, Bioorg. Med. Chem. 18 (2010) 1163–1170.
[64] A.H. Wang, J. Nathans, G. van der Marel, J.H. van Boom, A. Rich, Molecular structure of a double helical DNA fragment intercalator complex between deoxy CpG and a terpyridine platinum compound, Nature 276 (1978) 471–474.
[65] J.S. Casas, E.E. Castellano, J. Ellena, M.S. García-Tasende, M.L. Pérez-Parallé, A. Sánchez, A. Sánchez-González, J. Sordo, A. Touceda, New Pd(II) and Pt(II) complexes with N,S-chelated pyrazolonate ligands: molecular and supramolecular structure and preliminary study of their in vitro antitumoral activity, J. Inorg. Biochem. 102 (2008) 33–45.
[66] H.H. Repich, V.V. Orysykb, L.G. Palchykovska, S.I. Orysyka, Yu.L. Zborovskii,

O.V. Vasylchenko, O.V. Storozhuk, A.A. Bilukd, V.V. Nikulina, L.V. Garmanchuk, V.I. Pekhnyo, M.V. Vovk, Synthesis, spectral characterization of novel Pd(II), Pt(II) π-coordination compounds based on N-allylthioureas. Cytotoxic properties and DNA binding ability, J. Inorg. Biochem. 168 (2017) 98–106.

[67] T.A. al-Allaf, L.J. Rashan, Cis-and trans-platinum and palladium complexes: a comparative study review as antitumor agents, Boll. Chim. Farm. 140 (3) (2001) 205–210.

[68] Y.A. Al-Soud, H.H. Al-Sa'doni, H.A.S. Amajaour, K.S.M. Salih, M.S. Mubarak, N.A. Al-Masoudi, I.H. Jaber, Synthesis, characterization and anti-HIV and antitumor activities of new coumarin derivatives, Z. Naturforsch. 63b (2008) 83–89.

[69] R.I. Dragoslav, V.J. Verica, P.R. Gordana, A. Katarina, R. Biljana, H.T. Ljubica, V. Nenad, S. Slobodan, K. Olivera, T. Vladimir, R.T. Srecko, Synthesis, characterization and cytotoxicity of a new palladium(II) complex with a coumarine-derived ligand, Eur. J. Med. Chem. 74 (2014) 502–508.

[70] M.S. Nermien, M.M. Hany, A.E.H.K. Essam Shawky, S.M. Shymaa, M.E. Ahmed, Synthesis of 4H-chromene, coumarin, 12H-chromeno[2,3-d]pyrimidine derivatives and some of their antimicrobial and cytotoxicity activities, Eur. J. Med. Chem. 46 (2011) 765–772.